Enhanced luminescence of dyes-decorated ZIF-8 composite films via D-A interactions for white light emission

Qiufen Liu,[a] *Xuelei Chen,*[a] *Jiahao Wu,*[a] *Liming Zhang,*[a] *Guanjie He,*[b] *Shouqin Tian* *[a] *and Xiujian Zhao* [a]

[a] State Key Laboratory of Silicate Materials for Architectures, Wuhan University of Technology (WUT), No. 122, Luoshi Road, Wuhan 430070, P. R. China. E-mail: tiansq@whut.edu.cn.

[b] School of Engineering and Materials Science, Queen Mary University of London, Mile End Road, London E1 4NS, UK

KEYWORDS: H_3BTC-ZIF-8; white light emission; D-A interactions; enhanced quantum efficiency

ABSTRACT

Metal organic frameworks (MOFs) constructed by metal ions/clusters and organic linkers are used to encapsulate fluorescent guest species with aggregation-caused quenching (ACQ) effects to enhance fluorescence properties due to their porous structures and high specific surface areas. However, there would be a problem of size matching between MOFs pores and guest molecules sizes. In this paper, amorphous ZIF-8 was modified by carboxyl functional groups (H_3BTC-ZIF-8) via introducing the 1,2,4-benzenetricarbonic acid (H_3BTC) ligand into the ZIF-8 sol system. And the H_3BTC-ZIF-8 was used for organic fluorescent dyes rhodamine 6G (R6G) and coumarin 151 (C151) loading to prepare R6G/C151/H_3BTC-ZIF-8 composite films. A white-light-emitting composite film (R6G/C151/H_3BTC-ZIF-8) with a CIE coordinate of (0.323. 0.347) was successfully prepared by compounding fluorescent dyes (R6G and C151) with H_3BTC-modified ZIF-8, whose photoluminescence quantum yield (PLQY) can reach 64.0%. It was higher than the PLQY of the composite films prepared by crystalline-ZIF-8 (40.2%) or amorphous ZIF-8 without H_3BTC (48.0%) compounded with the same concentrations of dyes. The fluorescence enhancement was probably attributed to an increased amount of active sites of H_3BTC-modified ZIF-8 interacted with dyes C151 and R6G. This can form hydrogen bonds between H_3BTC-ZIF-8 and C151, and weak electron donor-acceptor (D-A) interactions between H_3BTC-ZIF-8 and R6G molecules, respectively, thus enhancing the interactions between dyes and ZIF-8 and reducing the ACQ effect existing between dye molecules. Therefore, this strategy could provide an important guidance to develop white light emissive materials.

1. Introduction

Solid white-light-emitting-diodes (WLED) are the most promising illumination sources because of their excellent luminescence properties like high luminous efficiency, high cycle durability, and environmental friendliness.[1-3] In general, a blue LED chip with a yellow phosphor $Y_3Al_5O_{12}:Ce^{3+}$ can fabricate a WLED, and the combination of individual of red, blue and green LED chips into a lamp also can achieve white light emission.[1,4-6] However, the synthesis of phosphors requires rigorous conditions and substantial energy cost. Moreover, the difference in the degradation rate between chips and phosphors may cause chromatic aberration and poor white light performance after reuse for many times.[6] In this sense, it is necessary to develop emerging luminescent materials. Up to now, many luminescent materials such as rare earth materials,[7-9] organic fluorescent dyes,[10-13] perovskites,[14-20] quantum dots,[21-24] metal organic frameworks (MOFs),[4,5,13] and carbon dots,[25-27] show great potentials in structure versatility, wavelength tunability and short luminescence lifetimes, and have been used in white LEDs.

Among these luminescent materials, metal organic frameworks (MOFs) constructing metal ions/clusters with organic ligands, have been promising inorganic-organic hybrid porous materials. Compared with other porous materials, MOFs exhibit high specific surface areas, adjustable pore sizes, and high degrees of functionalization.[28-30] Additionally, luminescent MOFs (LMOFs)[31] have attracted much attention to develop excellent luminescent functional materials in recent years due to their inherent luminescent centers of metal nodes/clusters such as rare earth cations, and chromophoric ligands.[32-35] On the other hand, many researchers have tried to encapsulate other luminescent materials like organic fluorescent dyes using MOFs to obtain composite materials,[1,33,36-40] which can exhibit better fluorescence performance.

Organic fluorescent dyes are one of main groups of luminescent materials, presenting good luminescent performance including large absorption coefficient, high quantum yields, and wide excitation band.[1,41] Unfortunately, most commercial organic fluorescent dyes often suffer from a non-radiative process due to strong aggregation-caused quenching (ACQ) effect between dye intermolecular when they are in solid states or highly concentrated solutions, which would greatly reduce fluorescence properties or generate even no fluorescence.[41,42] In this sense, encapsulating organic fluorescent dyes into MOFs was a good strategy to enhance luminescence performance and weaken ACQ effects between dyes. However, there would be a problem of size matching between MOFs pores and dye molecules. Hence, it is very important to select MOF materials with appropriate pore sizes to encapsulate corresponding dye molecules, which can effectively weaken the ACQ effect between dyes molecules. Therefore, there are still difficulties and limitations in using MOFs to encapsulate organic fluorescent dyes.

In our work, we provided a new method to combine fluorescent dyes with MOF materials, the MOF structure was modified with functional groups to enhance the interaction between dyes and MOFs, thus weakening the ACQ effect between dyes molecules and improving the fluorescence performance. Firstly, an amorphous ZIF-8 (one type of zeolitic imidazole frameworks, belonging to MOFs[43]) film with carboxyl functional groups modified was obtained by adding some H_3BTC into the ZIF-8 reaction system, and the optical band gap of the H_3BTC-modified ZIF-8 was decreased to 4.06 eV comparing with the amorphous ZIF-8 (E_g=5.17 eV). And a white-light-emitting composite film (R6G/C151/H_3BTC-ZIF-8) with a CIE coordinate of (0.323. 0.347) was successfully prepared by compounding fluorescent dyes (R6G and C151) with H_3BTC-modified ZIF-8, whose photoluminescence quantum yield can reach 64.0%. It was higher than the PLQY of the composite films prepared by crystalline ZIF-8 (40.2%) or amorphous ZIF-8 (48.0%)

compounded with the same concentrations of dyes. The results suggested that the interaction sites between dyes (C151 and R6G) and ZIF-8 can be increased by modifying the structure of ZIF-8 using additional ligands (H_3BTC), enhancing the interactions between dyes and ZIF-8, and reducing the ACQ effect between dyes molecules. Finally, better immobilization and dispersion of dye molecules in the H_3BTC-ZIF-8 film can be achieved to improve the whole fluorescence performance in the composite film.

2. Experiment Section

2.1. Materials

Zinc acetate dihydrate ($Zn(CH_3COO)_2 \cdot 2H_2O$, ≥99.9%, Shanghai China), 2-methylimidazole (Hmim, $C_4H_6N_2$, 99%, Sigma-Aldrich), 1,2,4-benzenetricarbonic acid (H_3BTC, $C_9H_6O_6$, Macklin), Ethanol (≥99.7%, Shanghai China), 7-amino-4-trifluoromethyl coumarin (C151, $C_{10}H_6F_3NO_2$, 99%, Aladdin), and Rhodamine 6G (R6G, $C_{28}H_{31}N_2O_3Cl$, WoKai) were used without further purification, and ultrapure water was obtained through the purified water system (He Tai).

2.2. Preparation of H_3BTC-ZIF-8 film and R6G/C151/H_3BTC-ZIF-8 composite film

2.2.1. Preparation of H_3BTC-ZIF-8 precursor sols

The preparation process of the H_3BTC-ZIF-8 precursor sol was similar to our previous work,[44] and specific preparation process was as followed. Firstly, H_3BTC ligands (0.75 mmol) and Hmim ligands (25 mmol) (The mole ratio of Hmim to H_3BTC was 100:3) were mixed in 2 mL ethanol, and then stirred at room temperature to ensure complete dissolution of H_3BTC powders. Afterwards, 10 mmol $Zn(CH_3COO)_2 \cdot 2H_2O$ powders were added into the well-mixed solution under the continuous stirring process. Finally, the steady transparent H_3BTC-ZIF-8 precursor sol was obtained.

2.2.2. Preparation of H_3BTC-ZIF-8 films

The H_3BTC-ZIF-8 precursor sol was coated on a clear quartz glass through a spin-coating method to obtain a H_3BTC-ZIF-8 wet film. Then, the H_3BTC-ZIF-8 wet film was cured on a hot plate. The specific curing procedure was at 60 °C for 30 mins firstly, increasing the temperature by 20 °C per 30 mins to 120 °C and maintaining for 5 h. Finally, the H_3BTC-ZIF-8 film was obtained. It is noteworthy that the amount of H_3BTC in the H_3BTC-ZIF-8 film can be controlled by changing the mole ratio of Hmim to H_3BTC in the H_3BTC-ZIF-8 precursor sol.

2.2.3. Preparation of R6G/C151/H_3BTC-ZIF-8 composite films

The H_3BTC-ZIF-8 precursor sol was used as the solvent to disperse organic fluorescent dyes C151 and R6G, in which the mole ratio of Hmim to H_3BTC was 100:3. Firstly, 0.005 mmol C151 and 0.005 mmol R6G powders were mixed and dissolved in 5 mL of the H_3BTC-ZIF-8 precursor sol to form a transparent composite sol (The concentration of C151 and R6G were both 0.001 mol/L). After that, the same method of preparation of H_3BTC-ZIF-8 films was used to prepare C151/R6G/H_3BTC-ZIF-8 composite films. Among them, the concentrations of C151 and R6G in the obtained composite films were stood for the concentrations in the composite sol due to the homogeneity of the sol. And the colour of emission could be controlled by the concentrations of C151 and R6G dyes in the sol.

2.3. Characterizations

The phase structures of obtained films were characterized by X-ray diffraction (XRD) adopting grazing incidence scanning with the Cu Kα radiation at a scanning rate of 0.02°·2θ/s. The morphology and film thicknesses of films were employed by a field-

emission scanning electron microscope (FESEM) with an equipment of energy disperse spectroscopy analysis (EDS). The functional groups in microstructures of obtained films were detected by Fourier transform infrared spectra (FTIR) in the mid-infrared spectral range from 4000 to 400 cm^{-1}. To characterize possible structure changes on the surface of the ZIF-8 films before and after compounding fluorescent dyes, X-ray photoelectron spectrometer (XPS) tests accompanied with the ultraviolet photoelectron spectroscopy (UPS) characterizations were performed. The UV-Vis absorption spectra were obtained using a UV-Vis spectrophotometer with the wavelength range from 200 to 800 nm. The photoluminescence spectra (PL) of all films were measured at room temperature with a fluorescence spectrophotometer. The PL quantum efficiency was measured using a UV-NIR absolute PLQY spectrometer (Quantaurus-QY Plus, Hamamatsu, Japan). The fluorescence lifetime decay curves of films were obtained with a time-resolved fluorescence spectrometer (Newport, USA), and the excitation light was pumped by a femtosecond laser.

3. Results and discussions

3.1. Structure characterizations

Figure S1 showed XRD patterns of ZIF-8 film without H_3BTC, H_3BTC-ZIF-8 film and R6G/C151/H_3BTC-ZIF-8 composite film synthesized by a sol-gel method. The results showed that all samples had a strong and broad peak at 15°, indicating the formation of amorphous ZIF-8 phase[44] both before and after adding the fluorescent dyes (R6G and C151). This may be that the amount of dyes added was too small to detect the change. In order to further demonstrate the prepared amorphous film was amorphous ZIF-8, the amorphous film without H_3BTC was heated to 140 °C for 1 h and then characterized by

XRD. The result was shown in Figure S2. It can be seen that obvious peaks of ZIF-8 crystal can be observed, indicating that the nucleation condition of ZIF-8 was not reached under our experimental temperature of 120 °C in our reaction system and thus the amorphous ZIF-8 was formed.

To observe morphologies of these films, FESEM characterizations were carried out shown in Figure S3. It can be seen from the Figure S3a that, the surface of the ZIF-8 film synthesized without H_3BTC ligand was smooth, and there were many small particles on the surface after magnification and average size of particles was approximately 50 nm. As for the H_3BTC-ZIF-8 film, particles on the surface of the prepared film are smaller shown in Figure S3e. Additionally, it cannot be seen particles on the surface of the R6G/C151/H_3BTC-ZIF-8 composite film (Figure S3h). The reason for this phenomenon may be that the addition of both H_3BTC and dyes (R6G and C151) may affect the coordination of Zn^{2+} with Hmim in the ZIF-8 skeleton, resulting in the difference in particle sizes. Moreover, the thicknesses of above three films were 6.91, 6.01 and 8.05 μm, respectively. To further explore the elemental distribution of the R6G/C151/H_3BTC-ZIF-8 composite film, element mapping has been employed shown in Figure S4. It can be seen from the result that elements of C, N, O, Zn and F were exhibited a uniform distribution, suggesting the homogeneity of the composite film.

To investigate the structural difference between ZIF-8 films and the R6G/C151/H_3BTC-ZIF-8 composite film, FTIR characterizations were performed shown in Figure 1. The absorption peak at 422 cm^{-1} was attributed to Zn-N stretching vibration, and the peak at ~678 cm^{-1} was the out-of-plane bending vibration of the organic ring. Peaks at ~753 and 1143 cm^{-1} belonged to =C-H bending vibrations. The peaks at ~995 cm^{-1} and ~1175 cm^{-1}

were corresponding to C=C-N twisting and C-N bending vibration, respectively. The peak at ~1015 cm^{-1} belonged to C-H out-of-plane bending vibration of CH_3.[45,46] And a broad absorption band at the range of 3200 to 2200 cm^{-1} indicated the existence of N-H stretching vibration due to protonated imidazole and the peak at ~3400 cm^{-1} was associated with O-H stretching vibration.[47-49] Additionally, the peak (1591 cm^{-1}) with the highest relative intensity is attributed to C=C/ C=N or C=O stretching vibration due to the presence of conjugated structures in Hmim or H_3BTC ligands.[50] These results indicated that ZIF-8 frameworks with protonated imidazole structures has been formed (Figure 1a). Moreover, a wide band at the range of 955~915 cm^{-1} was attributed to the out-of-plane deformation vibration of O-H, which was used to confirm the presence of COOH.[47] In this sense, the ZIF-8 has been modified by carboxyl groups successfully. Although no significant peak changes were observed after forming the R6G/C151/H_3BTC-ZIF-8 composite film, the relative strength of Zn-N, a key structure in the formation of ZIF-8 framework, had been decreased in the H_3BTC-ZIF-8 film in Figure 2I, comparing with out-of-plane bending vibration of =C-H of Hmim ($\gamma_{=C-H}$). The possible reason for this phenomenon was that H_3BTC may affect the coordination environment of ZIF-8 and eventually lead to a change in the number of N active sites used for coordination with Zn.

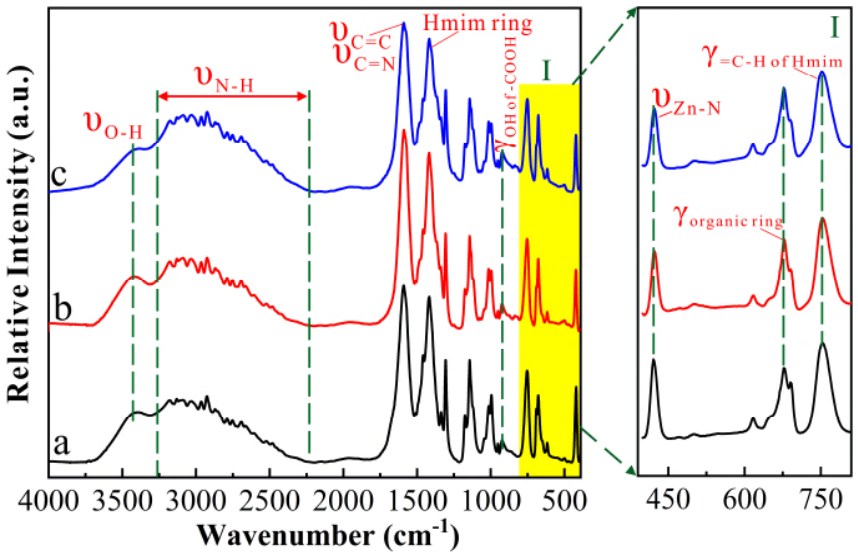

Figure 1 FTIR spectra of ZIF-8 film without H_3BTC (a), H_3BTC-ZIF-8 film (b), and R6G/C151/H_3BTC-ZIF-8 composite film (c). I. The enlarged FTIR spectra with a wavenumber range from 390 to 800 cm^{-1}.

To further investigate the role of the ligand H_3BTC in the formation of the ZIF-8 structure, sols prepared in different mole ratios of Hmim to H_3BTC without zinc salts and ZIF-8 films prepared in different mole ratios of Hmim to H_3BTC in the system in the presence of zinc salts were further characterized by FTIR. Prior to this, ligands Hmim and H_3BTC were also characterized by FTIR, and results were shown in Table S1 and S2 respectively.[44,51] In general, both Hmim and H_3BTC are easy to form intermolecular hydrogen bonds in solid state.[45,51] However, the types of intermolecular hydrogen bonds would be changed after adding H_3BTC into Hmim, results have been shown in Figure S5. It can be seen that the vibrational peaks of both Hmim and H_3BTC were existed in the sol samples mixed Hmim with H_3BTC, and the absorption peaks due to the resonance between υ_{N-H} and $\gamma_{N-H\cdots N}$ [52] moved to high wavenumber with the increase of H_3BTC. Also, the proportion of hydrogen bonds formed between Hmim molecules was decreased

in terms of the peak shape of the formed hydrogen bonds (2200-3200 cm^{-1}).[48] The possible reason for this phenomenon was the formation of hydrogen bonding interactions between Hmim and H_3BTC, creating new hydrogen bonding species, i.e. N-H···O or O-H···N hydrogen bonds. Additionally, FTIR spectra (Figure S6) of ZIF-8 films prepared with different mole ratios of Hmim to H_3BTC showed that the relative intensity of stretching vibration of Zn-N decreased with the increase of H_3BTC (Figure S6a). And as the mole ratio increased, the deformation vibration of =C-H from benzene ring gradually became obvious (Figure S6b). In Figure S6c, the vibrations of characteristic functional groups from H_3BTC increased with the increase of the mole ratio, and the absorption peak at ~1590 cm^{-1} widened due to the increased conjugated system. These results have indicated that H_3BTC modified ZIF-8 was indeed formed and the interaction between H_3BTC and Hmim inhibited the formation of the ZIF-8 structure to a certain extent. On the other hand, the presence of a certain number of carboxyl functional groups on the H_3BTC-modified ZIF-8 provided some convenience for following dyes loading. In a word, the addition of H_3BTC ligands to the ZIF-8 synthesis could modulate the coordination of Zn with Hmim and also modify the ZIF-8 structure with functional groups of -COOH. It was worth noting that the addition of H_3BTC shouldn't be too much, which would lead to serious inhibition of Zn coordinated with Hmim, and eventually failed to form the ZIF-8 skeleton resulting in poor stability.

Additionally, ZIF-8 sols and film samples at different curing temperatures after film formation were also characterized by FTIR, as shown in Figure S7. It can be seen from the figure that both in the system without H_3BTC (Figure S7a) and the system containing H_3BTC ligands (Figure S7b), the relative intensity of Zn-N stretching vibration in formed

sols was very small, marked yellow area 1 and 5, indicating that the ZIF-8 skeleton was almost not formed in sols. As the increasing of the curing temperature, the intensity of the Zn-N stretching vibration was significantly enhanced, implying the gradual formation of the ZIF-8 structure. The area 2 and 6 in Figure S7 showed the out-of-plane deformation vibration of O-H from -COOH and the relative strength was decreased with the increasing of the curing temperature. Also, the absorption peaks due to the resonance between $\upsilon_{N\text{-}H}$ and $\gamma_{N\text{-}H\cdots N}$ (area 3 and area 7), and protonated imidazole (area 4 and area 8) were disappeared and decreased, respectively, indicating reduced interactions between imidazole molecules. The reason for these results may be that increasing temperature can not only promote the volatilization of solvent molecules in wet films, but also destroy part of hydrogen bond interactions between imidazole molecules or between imidazole molecules and acidic small molecules (acetic acid or H_3BTC), which would promote the coordination of Zn and imidazole, and resulting in the formation of the ZIF-8 structure. In this sense, increasing temperature was favourable to the formation of ZIF-8. Furthermore, the relative intensity of Zn-N in the ZIF-8 film without H_3BTC was higher than that of the ZIF-8 film with H_3BTC, suggesting that the ligand H_3BTC modulated the coordination environment of ZIF-8.

To demonstrate that Zn^{2+} didn't coordinate with H_3BTC and to verify our previous results, XPS characterizations were performed on ZIF-8 films synthesized with/without H_3BTC and H_3BTC powders. XPS survey spectra showed the presence of Zn, C, N, O elements in both the ZIF-8 film without H_3BTC (Figure S8c) and H_3BTC-ZIF-8 film (Figure S8a). Because there was no O element in the ZIF-8 structure, the O element was mainly derived from acid molecules. Additionally, the contents of C and O relative to Zn

increased significantly, suggesting that H_3BTC-modified ZIF-8 structures have been formed. And Zn 2p spectra of ZIF-8 without H_3BTC (Figure S8d) had two peaks centred at ~1045 and ~1022 eV, corresponding with binding energies of Zn $2p^{1/2}$ and Zn $2p^{3/2}$, respectively.[53] It was worth noting that the two peaks of Zn 2p moved towards the higher binding energy by ~1 eV for the H_3BTC-ZIF-8 film comparing with the ZIF-8 film without H_3BTC modified, indicating that there may be some interaction between ZIF-8 and H_3BTC resulting in the peak offset of Zn 2p. The XPS high resolution of C1s spectra of ZIF-8 films (Figure 2a and 2d) through peak fitting contained four types of the carbon environment with binding energy values of ~284.8 eV, ~285.8 eV, 286.8 eV and ~288.5 eV, which mainly originated from the graphitic carbon/C-sp^3, C=C, C-O and C=N/C=O, respectively.[44,54] When adding H_3BTC ligand to the ZIF-8 system, the relative intensity of C=N/C=O in Figure 2d was increased, indicating the successful synthesis of carboxyl-modified ZIF-8. Furthermore, XPS high resolution of N1s (Figure 2b and 2e) and O1s (Figure 2c and 2f) spectra were important for the proof of the coordination in ZIF-8, and the results indicated that the relative intensity of protonated N (N-H) in the H_3BTC-ZIF-8 film was significantly enhanced, comparing with the ZIF-8 film synthesized without H_3BTC. This suggested that adding H_3BTC inhibited the deprotonation of Hmim, which eventually leaded to a decrease in N sites coordinated with Zn. At the same time, peaks of O1s indicated the presence of oxygen only from small molecules such as H_3BTC, CH_3COOH, H_2O and CO_2, and no coordination of O with Zn was found, which proved that H_3BTC only changed the N environment of Zn coordinated with Hmim and did not participate in the formation of ZIF-8 structures.

In summary, the addition of H_3BTC ligand to the ZIF-8 synthesis system can regulate the N environment of ZIF-8 and modify carboxyl functional groups on ZIF-8 structure. Furthermore, it does not participate in the coordination with Zn.

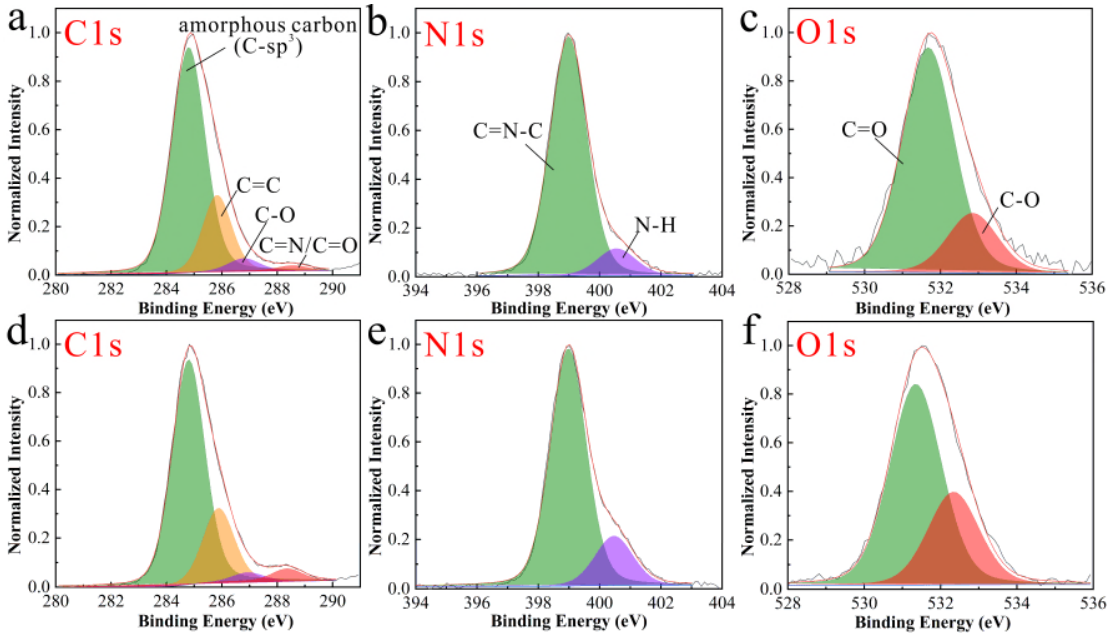

Figure 2 XPS high resolution C1s spectra (a and d), N1s spectra (b and e) and O1s spectra (c and f) of ZIF-8 films without H_3BTC (a-c) and H_3BTC-ZIF-8 film (d-f).

Next, interactions between fluorescent dyes (R6G and C151) and H_3BTC-ZIF-8 in the R6G/C151/H_3BTC-ZIF-8 composite film was investigated. Based on others' works previously, there were several main interactions among MOF hosts and guest species, including electrostatic interaction, π-π interaction, ion exchange, hydrogen bonds, and so on.[55] Firstly, π-π interactions have been formed between H_3BTC-ZIF-8 and dyes due to the existence of π conjugation systems in both H_3BTC-ZIF-8 and dye molecules (R6G and C151).[47,56] On the other hand, to investigate whether there were other interactions between H_3BTC-ZIF-8 and dye molecules, FTIR characterizations were performed on

composite films with different concentrations of single fluorescent dyes and results have shown in Figure S10. As seen from Figure S10a, when the concentration of R6G was 0.001 mol/L, the relative intensity of Zn-N had little changes compared with the H_3BTC-ZIF-8 film without dyes. While the concentration of R6G was up to 0.01 mol/L, the relative intensity of Zn-N was increased. And the stretching vibration of O-H also weakened with the increase of R6G. Since R6G is a cationic dye ($R6G^+$), it can serve as an electron acceptor, and there are carboxyl functional groups in H_3BTC-ZIF-8 structure acting as an electron donor.[57] In this sense, the donor-acceptor (D-A) interactions may exist between H_3BTC-ZIF-8 and R6G, which weakened the inhibition of H_3BTC on ZIF-8 structure resulting in an enhanced coordination degree between Zn and Hmim. However, when the concentration of R6G was too high, its fluorescence performance would be decreased because of ACQ effects. In this sense, the concentration of R6G incorporation should not be too high.

A similar phenomenon was observed in C151/H_3BTC-ZIF-8 composite films shown in Figure S10b, and results showed that the relative intensity of Zn-N stretching vibrations increased more obviously with the increasing concentration of C151 comparing with the R6G/H_3BTC-ZIF-8 composite film. Moreover, the stretching vibration intensity of O-H was weakened more clearly, suggesting that the fluorescent dye C151 was more easily to promote the coordination of Zn with Hmim in dyes/H_3BTC-ZIF-8 composite film comparing with R6G. Since C151 has three types of structures that can form hydrogen bonds which include participation of the amino nitrogen (N), the carbonyl oxygen (C=O), and amino hydrogen (N-H),[58] hence, the possible reason for this phenomenon was the existence of hydrogen bonding interactions between N-H functional groups in C151 and

carboxyl groups (-COOH) in H_3BTC-ZIF-8, and protonated N sites (N-H) in ZIF-8 could also form N-H···O=C hydrogen bonds with the carbonyl oxygen of C151, which both can weaken the inhibitory effect of H_3BTC on the formation of the ZIF-8 framework, and finally the interplay of multiple roles makes the whole system more stable.[56,59]

In order to further prove that dyes R6G and C151 have attenuated the inhibitory effect of H_3BTC on ZIF-8, XPS high resolution N1s characterizations of dyes/H_3BTC-ZIF-8 composite films were performed, as shown in Figure 3. It can be seen from the figure that when the concentration of R6G was 0.001 mol/L, the relative strength of protonated N was decreased compared with the H_3BTC-ZIF-8 film (Figure 3a and 3b), indicating that R6G molecules formed weak D-A interactions with the electron donor O in H_3BTC-modified ZIF-8 that weakened the inhibition effect of Hmim deprotonation by H_3BTC. This interaction resulted in a decrease in the proportion of protonated N sites, corresponding to a relative decrease in the proportion of N-H in Figure 3b. Additionally, when the concentration of C151 was 0.001 mol/L (Figure 3c), the relative intensity of N-H was also significantly weakened compared with that of the H_3BTC-ZIF-8 film, indicating that the hydrogen bonds formed between C151 and H_3BTC-ZIF-8 could effectively weaken the inhibitory effect of H_3BTC on deprotonation of Hmim, consistent with the FTIR result (Figure S10b).

When the concentration of both R6G and C151 used to prepare a R6G/C151/H_3BTC-ZIF-8 composite film was 0.001 mol/L, there was a certain competition between them due to the limited and overlapped action sites of H_3BTC-ZIF-8, which made the degree of the interaction between dyes (R6G and C151) and H_3BTC-ZIF-8 changed. Therefore, it was possible to optimize the distribution of R6G and C151 in the H_3BTC-ZIF-8 structure

through modulating the amount carboxyl functional groups of ZIF-8 after H_3BTC modification, which can effectively reduce the ACQ effect of dye molecules and finally obtain a composite film with excellent fluorescence performance.

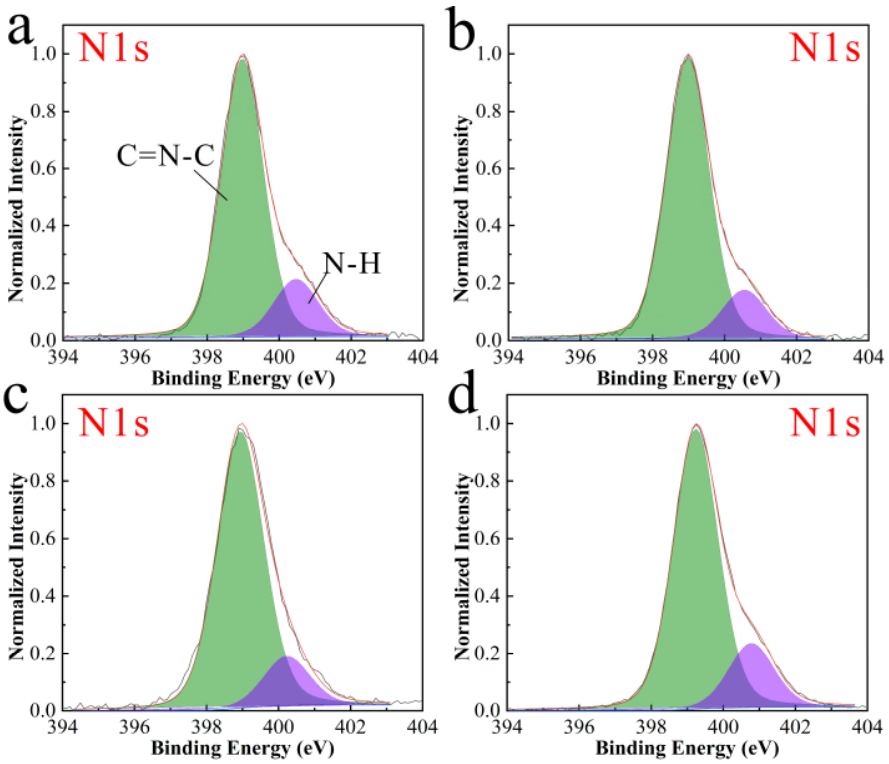

Figure 3 XPS high resolution N1s spectra of the H_3BTC-ZIF-8 film without dyes (a), the R6G/H_3BTC-ZIF-8 film with a concentration of R6G of 0.001 mol/L (b), the C151/H_3BTC-ZIF-8 film with a concentration of C151 of 0.001 mol/L (c), and the R6G/C151/H_3BTC-ZIF-8 composite film with dyes (both R6G and C151) concentrations of 0.001 mol/L (d).

3.2. Structure formation mechanism

In this work, the solid-state white light composite film with high fluorescence quantum efficiency was successfully prepared by the interaction of the H_3BTC-modified ZIF-8 structure with fluorescent dyes R6G and C151. The possible mechanism of interactions

between dyes (R6G and C151) and H_3BTC-ZIF-8 was shown in Figure 4. In a ZIF-8 sol system without H_3BTC ligands, the mole ratio of Hmim to Zn source ($Zn(CH_3COO)_2 \cdot 2H_2O$) was relatively low (2.5:1), and small acidic molecules CH_3COOH produced by the hydrolysis of Zn source inhibited the deprotonation process of Hmim, which would make a low degree of coordination between Zn and Hmim in the sol. Specific reaction equations are as follows:[44]

$$Zn(CH_3COO)_2 + 2H_2O \leftrightarrow Zn(OH)_2 + 2CH_3COOH \quad (1)$$

$$Zn^{2+} + nHmim \rightarrow Zn(Hmim)_n^{2+} \quad (2)$$

$$Zn(Hmim)_n^{2+} + Hmim \rightarrow Zn(Hmim)_{n-1}(mim)^{+} + H_2mim^{+} \quad (3)$$

$$H_2mim^{+} + OH^{-} \leftrightarrow Hmim + H_2O \quad (4)$$

When the sol forms solid films through a spin-coating method and curing, the inhibition effect on Hmim deprotonation was weakened because of the volatilization of some small molecules acetic acid during the curing process, which promoted the coordination of Zn with imidazole to form the ZIF-8 skeleton. However, it is difficult to remove all acetic acid molecules due to the existence of hydrogen bonds between CH_3COOH and protonated N (N-H) of imidazole.[44] Hence, some acetic acid existed in the ZIF-8 film, which was consistent with Figure 1 and Figure S7a. When a small amount of H_3BTC was added to the ZIF-8 sol, more carboxyl functional groups present in H_3BTC formed a strong hydrogen bonds (N-H···O and N···H-O) with N sites in Hmim, and these were not easily destroyed during curing at low temperatures (120 °C). Therefore, some hydrogen bonds and carboxyl functional groups have been preserved in the H_3BTC-ZIF-8 after curing and forming the film. Since the mole ratio of H_3BTC relative to Hmim was very small (3:100), and also, the system was under acidic conditions, in this sense, there would

be protonated N and carboxyl functional groups in the film, which facilitated interactions with fluorescence dye molecules. In a R6G/H_3BTC-ZIF-8 composite film at a low concentration of R6G, R6G molecules presented a better dispersion in the ZIF-8 structure, and the interaction between them was dominated by π-π stacking because of the presence of a large number of π conjugation systems both in ZIF-8 and R6G molecules.[55] Moreover, since R6G molecules belong to cationic dyes, they can act as electron acceptors to form D-A interactions with electron-rich structures (-COOH) in H_3BTC-ZIF-8, as shown in Figure 4. However, the relatively large size (16.0 × 8.0 Å)[60] of single R6G molecule made the D-A interaction weak, and R6G molecules were not completely highly dispersed in the H_3BTC-ZIF-8 structure, so there was also H-aggregate between R6G molecules resulting in ACQ effects.[39,61] When the concentration of R6G gradually increased, its π-conjugated structures gradually increased, which led to an enhanced π-π stacking interaction between H_3BTC-ZIF-8 and R6G. At the same time, the limited numbers of active sites on ZIF-8 molecules and the existence of stereo-hindrance effects would enhance R6G intermolecular interactions and gradually enhance the ACQ effect, and finally the fluorescence performance would be weakened.

On the other hand, in the C151/H_3BTC-ZIF-8 composite film, when the concentration of C151 was low, it could keep well interaction with the H_3BTC-ZIF-8 due to its small molecular size (8.0 × 11.0 Å)[13] and forming hydrogen bonds, and the existence of π conjugation system. These interactions would make C151 highly and stably dispersed in the H_3BTC-ZIF-8 film. When the concentration of C151 was increased, part of C151 could only exist in the ZIF-8 structure by intermolecular interaction due to the saturation of the interaction between C151 and H_3BTC-ZIF-8, which would enhance the ACQ effect

between C151 molecules shown in Figure 4. When adding the two dyes into the H_3BTC-ZIF-8 synthetic system, they would compete with each other for the overlapped H_3BTC-ZIF-8 active sites. Since H_3BTC ligands can regulate numbers of interaction sites with dyes, the reasonable regulation of ZIF-8 structures by H_3BTC may reduce the ACQ effect of C151 and R6G in the composite structure to bring out their respective maximum fluorescence performance.

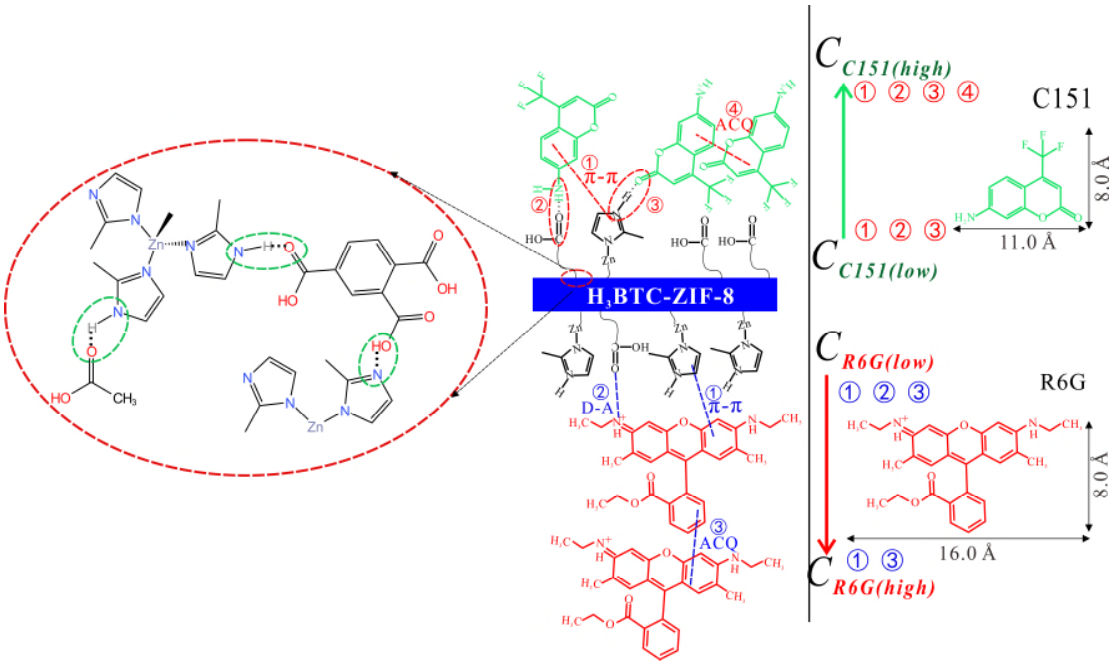

Figure 4 A possible structure formation mechanism illustration of the R6G/C151/H_3BTC-ZIF-8 composite film.

3.3. Luminescent properties

In order to explore the luminescent properties of the R6G/C151/H_3BTC-ZIF-8 composite film, firstly, the UV-Vis absorption spectra of ZIF-8 films and the R6G/C151/H_3BTC-ZIF-8 composite film have been employed shown in Figure S11. It

can be seen from the results that all films exhibited strong absorption edges in the ultraviolet region, and it was obvious that the absorption edge of the H_3BTC-ZIF-8 film moved from ~240 nm to ~305 nm comparing with the ZIF-8 film. Furthermore, the intensities of the absorption peaks at ~390 nm and ~540 nm of the R6G/C151/H_3BTC-ZIF-8 composite film increased slightly after the dye molecules were compounded. In order to further investigate origins of these absorption differences among these films, the UV-Vis absorption spectra of reactants including ligands and dyes used have been characterized (Figure S12). Results have shown that the absorption edge of the ZIF-8 film without H_3BTC at ~240 nm was from the imidazole Hmim ligand. And the absorption edge of H_3BTC was approximately 350 nm, which may be the reason for the movement of absorption edge between ZIF-8 film without H_3BTC and H_3BTC-ZIF-8 film. Similarly, the peaks at ~393 nm and ~545 nm in the R6G/C151/H_3BTC-ZIF-8 composite film originated from the organic fluorochromes C151 and R6G, respectively. Interestingly, in the R6G/C151/H_3BTC-ZIF-8 composite, the relative intensity of the electronic vibrational shoulder at 500 nm (0.305) originated from the formation of different types of dimers[62] comparing with the peak centred at 545 nm was significantly smaller than that of the single dye R6G (0.732), indicating that the formation of the composite film combining dyes with ZIF-8, to a certain extent, can weaken the ACQ effect of dyes and improve fluorescence performances.

On the other hand, the emission spectra of ZIF-8 films, the R6G/C151/H_3BTC-ZIF-8 composite film, and fluorescent dyes R6G and C151 at room temperature have been examined to determine the luminescent property of the dyes/H_3BTC-ZIF-8 composite film in Figure 5a. It can be seen that fluorescence emission peaks of C151 and R6G at an

excitation wavelength of 365 nm were at 470 and 568 nm, respectively. There was almost no change in blue emission (443 nm) between the ZIF-8 film and H_3BTC-ZIF-8 film, indicating that H_3BTC did not change the main structure of ZIF-8.

Furthermore, the R6G/C151/H_3BTC-ZIF-8 composite film was obtained by adding fluorescence dyes R6G and C151 to the H_3BTC-ZIF-8 synthesis. And two fluorescent emission peaks (~450 and ~570 nm) are attributed to the emission peaks of ZIF-8, C151 and R6G superimposed on each other.

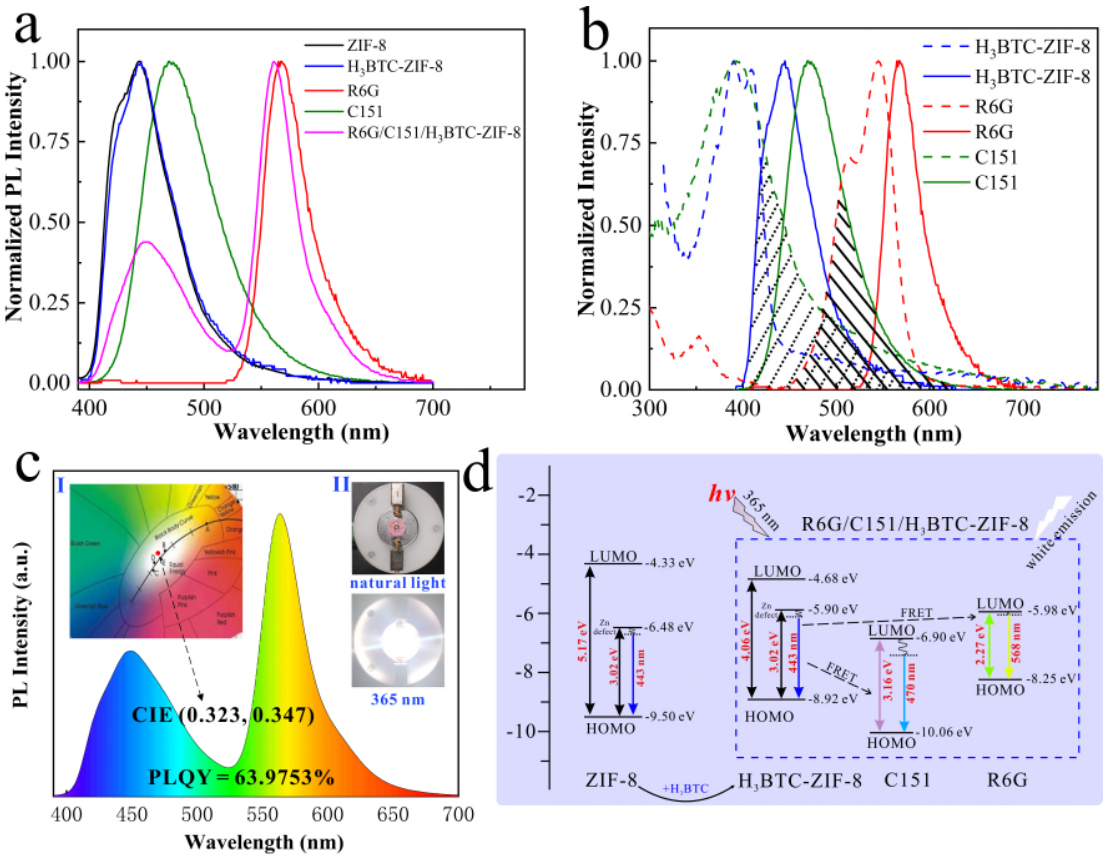

Figure 5 (a) Normalized PL spectra (λ_{ex}=365 nm) of dyes (R6G and C151), ZIF-8 films H_3BTC-ZIF-8 film and R6G/C151/H_3BTC-ZIF-8 composite film; (b) Emission spectra (solid lines) and absorbance spectra (dotted lines) of H_3BTC-ZIF-8 and dyes. (The black dotted line shaded area for the overlap of the emission spectrum of H_3BTC-ZIF-8 and the absorbance spectrum of C151, and the black solid line shaded area for the overlap of the emission spectrum of H_3BTC-ZIF-8/

C151 and the absorbance spectrum of R6G.) (c) The emission spectrum of the R6G/C151/H_3BTC-ZIF-8 composite film (λ_{ex}=365 nm). I: CIE chromaticity coordinates (0.323, 0.347), II: photographs of the R6G/C151/H_3BTC-ZIF-8 composite film upon the natural light and UV-365 nm, respectively. (d) A schematic diagram of R6G/C151/ZIF-8 composite film with white light emission prepared with H_3BTC-modified ZIF-8.

To investigate the possible resonance energy transfer phenomenon among H_3BTC-ZIF-8, C151 and R6G, their absorption and emission spectra were characterized as shown in Figure 5b. The shaded parts present in the figure between H_3BTC-ZIF-8 and C151, and between H_3BTC-ZIF-8/C151 and R6G may have satisfied the Förster resonance energy transfer (FRET)[44,63] from ZIF-8 to C151, and from ZIF-8/C151 to R6G, respectively, which was beneficial to improve the fluorescence performance of dyes. However, the overlap of the absorption and emission spectra of the individual material indicated the existence of self-absorption phenomena, which would cause an unavoidable weakening of the fluorescence performance.

Moreover, absolute photoluminescence quantum yields (PLQYs) of the R6G/C151/H_3BTC-ZIF-8 and R6G/C151/ZIF-8 composite films without H_3BTC modified have been measured and results were shown in Figure S13. It can be seen that the PLQY of the R6G/C151/H_3BTC-ZIF-8 composite film (64.0%) was higher than that of the R6G/C151/ZIF-8 composite film (48.0%) without H_3BTC under the condition of the same concentrations of dyes. Also, a composite film consisting of crystalline ZIF-8 and the same dyes was prepared using the same method and characterized by XRD and PLQY, as shown in Figure S14, suggesting its low quantum yield (40.2%). These results demonstrated that the obtained R6G/C151/H_3BTC-ZIF-8 composite film prepared by using H_3BTC-modified ZIF-8 was more favourable to the interaction between ZIF-8 and dyes, which effectively reduced the ACQ effect between dyes molecules and improved the

fluorescence performance of the composite film. And the composite film showed a cold white light emission with CIE coordinates of (0.323, 0.347) shown in Figure 5c, and its fluorescent lifetime (Figure S15) exhibited 5.41 and 2.46 ns for the peaks of 560 and 450 nm, respectively. Additionally, the correlated colour temperature (CCT) of the R6G/C151/H_3BTC-ZIF-8 composite film was 5908 K according to the relevant calculation formula of CCT (CCT = 437×N×N×N+3601×N×N-6861×N+5514.31, N=(x-0.332)/(y-0.1858), x and y are CIE coordinates.). Moreover, some previous works on fluorescence properties of composite materials prepared based on MOFs encapsulating fluorescent dyes, are summarized in Table 1. It could be seen that this approach of using functional groups modified amorphous MOF structures compounded with fluorescent dyes has an obvious advantage in improving fluorescence efficiency for the development of solid-state white light materials.

To evaluate the applicability of the R6G/C151/H_3BTC-ZIF-8 composite film for practical application, its thermostability and photostability were investigated. The results of thermal stability indicated that the fluorescence relative intensities of the emission peaks at 562 and 445 nm) of the R6G/C151/H_3BTC-ZIF-8 composite film can be maintained basically after heating at 100 ℃ for different times (Figure S16). However, the initial values of the spectrum differed significantly from other values due to insufficient preheating time of the light source. Meanwhile, the emission spectra of the R6G/C151/H_3BTC-ZIF-8 composite film was recorded after different exposure times irradiated by 365 nm UV light (Figure S17), indicating good photostability.

In addition, the luminescent properties of R6G/H_3BTC-ZIF-8 and C151/H_3BTC-ZIF-8 composite films prepared by compounding H_3BTC-ZIF-8 with different concentrations of single dye were investigated and results were shown in Figure 6. In Figure 6a, as the

concentration of R6G in the R6G/H_3BTC-ZIF-8 composite film increased, the fluorescence intensity derived from R6G was stronger excited at 365 nm, corresponding to the CIE spectrum colour gradually shifting from blue to orange-yellow (Figure 6c). And fluorescence quantum yields (Figure 6e) of R6G/H_3BTC-ZIF-8 composite films showed a trend of increasing (from 57.1% to 68.8%) and then decreasing (from 68.8% to 44.8%) with the increase of the R6G concentration, indicating that the ACQ effect of R6G molecules became obvious at higher concentrations. Meanwhile, a similar result was also observed in C151/H_3BTC-ZIF-8 composite films. As the C151 content gradually increased, the blue-green emission intensity of C151 displayed an incremental enhancement (Figure 6b). And PLQYs of C151/H_3BTC-ZIF-8 composite films were ranged from 47.1% to 67.0% (Figure 6f). In this sense, H_3BTC-modified ZIF-8 compounding fluorescence dyes R6G and C151 can effectively improve the fluorescence performance of the dyes.

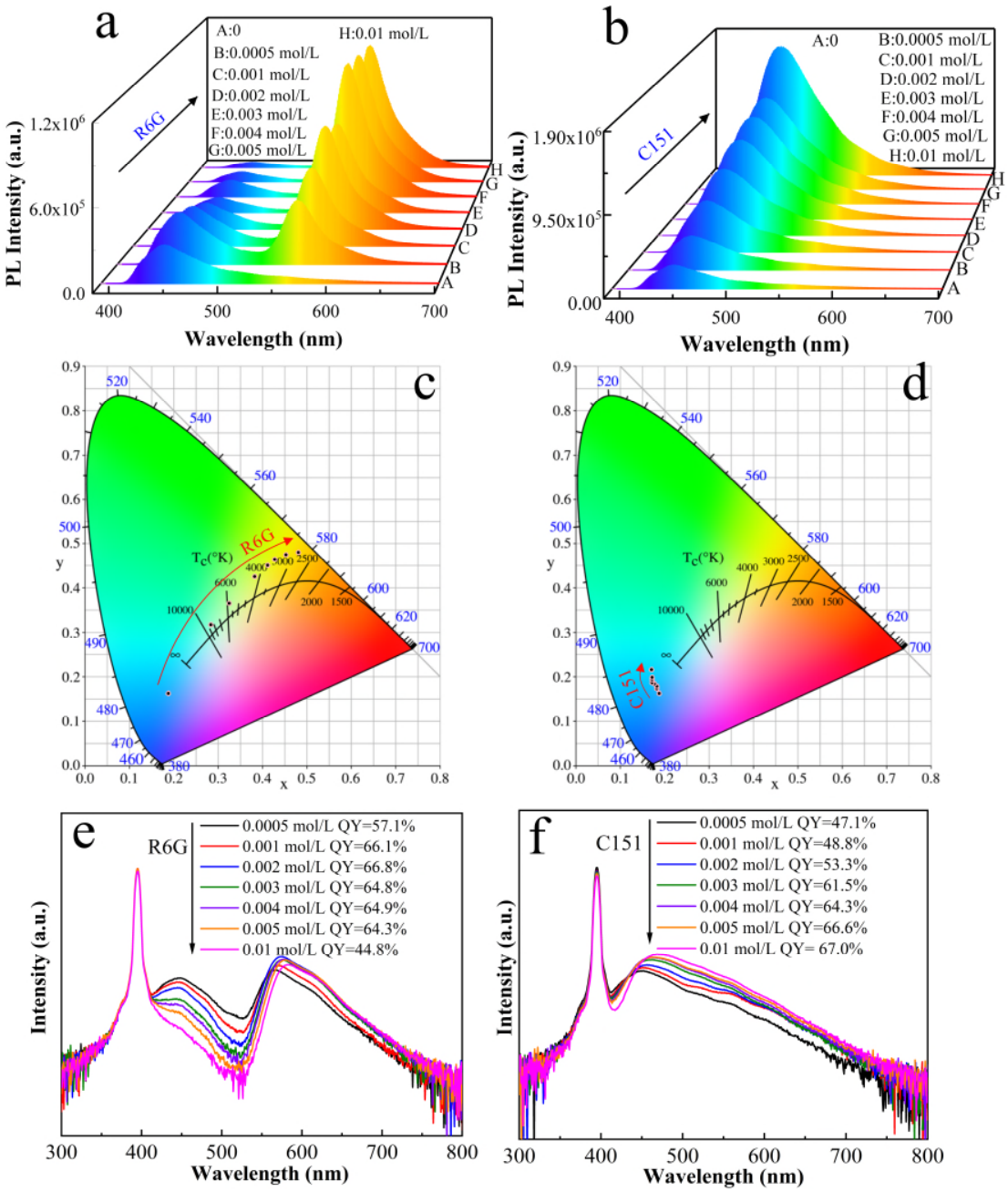

Figure 6 The emission spectra (λ_{ex}=365 nm) of R6G/H_3BTC-ZIF-8 composite films with different concentrations of R6G (a) and C151/H_3BTC-ZIF-8 composite films with different concentrations of C151 (b). CIE coordinates (λ_{ex}=365 nm) of R6G/H_3BTC-ZIF-8 composite films (c) and C151/H_3BTC- ZIF-8 composite films (d) at ambient temperature. PLQYs of

R6G/H_3BTC- ZIF-8 composite films (e) and C151/H_3BTC-ZIF-8 composite films (f), (λ_{ex}=395 nm).

Table 1 Summary of the fluorescence properties of various dyes@MOF composite materials.

materials	CIE (x, y)	emission color	PLQY	CCT (K)	references
C151@ZIF-8^2:F@ZIF-8^2:RB@ZIF-82 composite powders	0.32, 0.34	white	—	—	13
NKU-114@DSM/AF/9-AA	0.34, 0.32	white	42.07%	5101	41
HSB-W⊃DCM/C6a/CBS-127	0.31, 0.32	white	26.0%	6638	11
ZIF-8⊃pm546/pm605/SRh101	0.465, 0.413	white	52.5%	2642	64
CD-MOF⊃7-HCm@FL@RhB	0.35, 0.32	white	—	—	36
ZJU-28⊃Cou-6/R6G/R101	0.36, 0.34	white	82.9%	4446	65
DSM@PCN-128W	0.34, 0.33	white	21.2%	5525	12
Rh110@bio-MOF-1	0.3111, 0.3382	yellow-green	79%	6981	1
RhB^+@LIFM-WZ-6	0.33, 0.35	white	9.8%	4745	57
TPPA+ R6G@NKU-110	0.33, 0.34	white	49.1%	—	66
R6G/C151/H_3BTC-ZIF-8 film	0.323, 0.347	white	64.0%	5908	this work

3.4. The possible luminescent performance improvement mechanism

To uncover the relationship between fluorescent dyes (R6G and C151) and H_3BTC-ZIF-8, and the energy transfer among them, UPS characterizations of the dyes and ZIF-8 were performed, as shown in Figure S18. Additionally, the optical band gaps of dyes (R6G and C151) and ZIF-8 were calculated combining the corresponding absorption spectra. The specific schematic diagram was shown in Figure 5d. As can be seen in Figure 5d, the highest occupied molecular orbital (HOMO) levels located at -9.50, -8.92, -10.06, -8.25 eV and the lowest unoccupied molecular orbital (LUMO) levels located at -4.33, -4.68, -6.90, -5.98 eV for the ZIF-8, H_3BTC-ZIF-8, C151, and R6G, respectively. According to the optical band gap of the ZIF-8 (Eg=5.17 eV), 365 nm light can provide a photo energy of ~3.40 eV, not enough to excite electrons in the ZIF-8 to transfer. In this sense, the blue emission produced by 365 nm excitation was derived from the defect luminescence (Zn defect) in the ZIF-8 structure[44]. When the ZIF-8 was modified by H_3BTC with carboxyl functional groups, the HOMO-LUMO gap of the obtained H_3BTC-ZIF-8 was reduced from 5.17 eV to 4.06 eV, and also, the HOMO level was increased by 0.58 eV, indicating that the electrons were more easily excited. After forming a composite structure of R6G/C151/H_3BTC-ZIF-8 by combining the fluorescent dyes C151 and R6G with H_3BTC-ZIF-8, the inherent HOMO-to-LUMO energy transfer of H_3BTC-ZIF-8, C151, and R6G shows fluorescence emissions of 443, 470, 568 nm, respectively. Additionally, two types of possible FRET may exist in the composite structure, i.e. energy transfer from H_3BTC-ZIF-8 to C151 and from H_3BTC-ZIF-8 to R6G according to positions of LUMOs.[67] When the fluorescence produced by these energy transfers reaches the equilibrium emission of forming white light, white light would be obtained.

4. Conclusions

In summary, the R6G/C151/H_3BTC-ZIF-8 amorphous composite film with white light emission was successfully synthesized by using H_3BTC-modified amorphous ZIF-8 in combination with fluorescence dyes R6G and C151, exhibiting a high PLQY of ~64%. It was higher than the PLQY of the composite films prepared by crystalline ZIF-8 (40.2%) or amorphous ZIF-8 (48.0%) compounded with the same concentrations of dyes. The possible reason for this phenomenon is that there are carboxyl functional groups existed in H_3BTC-ZIF-8 structures increasing effectively active sites for interaction with dyes, which can form hydrogen bonds with C151 and weak D-A interactions with R6G molecules, thus enhancing the interactions between dyes and ZIF-8, and reducing the ACQ effect between dye molecules. Ultimately, the overall fluorescence performance of the composite film has been improved. This strategy by using functional groups modified amorphous MOF structures to synthesize composite materials has a significance for the development of luminescent materials in the application of solid white light.

AUTHOR INFORMATION

Corresponding Author

Shouqin Tian - *State Key Laboratory of Silicate Materials for Architectures, Wuhan University of Technology (WUT), No. 122, Luoshi Road, Wuhan 430070, P. R. China. E-mail: tiansq@whut.edu.cn.*

Authors

Qiufen Liu - *State Key Laboratory of Silicate Materials for Architectures, Wuhan University of Technology (WUT), No. 122, Luoshi Road, Wuhan 430070, P. R. China.*

Xuelei Chen - *State Key Laboratory of Silicate Materials for Architectures, Wuhan University of Technology (WUT), No. 122, Luoshi Road, Wuhan 430070, P. R. China.*

Jiahao Wu - *State Key Laboratory of Silicate Materials for Architectures, Wuhan University of Technology (WUT), No. 122, Luoshi Road, Wuhan 430070, P. R. China.*

Liming Zhang - *State Key Laboratory of Silicate Materials for Architectures, Wuhan University of Technology (WUT), No. 122, Luoshi Road, Wuhan 430070, P. R. China.*

Guanjie He - *School of Engineering and Materials Science, Queen Mary University of London, Mile End Road, London E1 4NS, UK*

Xiujian Zhao - *State Key Laboratory of Silicate Materials for Architectures, Wuhan University of Technology (WUT), No. 122, Luoshi Road, Wuhan 430070, P. R. China.*

Author Contributions

The manuscript was written through contributions of all authors. All authors have given approval to the final version of the manuscript.

Conflicts of interest

There are no conflicts to declare.

Acknowledgements

This work was supported by the National Natural Science Foundation of China (Grant No. 51772229), the 111 project (No. B18038), the National Key R&D Program of China (No. 2017YFE0192600), Key R&D Project of Hubei Province (No.2020BAB061), National innovation and entrepreneurship training program for college students, Open Foundation of the State Key Laboratory of Silicate Materials for Architectures at WUT (No. SYSJJ2021-05 and SYSJJ2022-01), Open Research Fund Program of Science and Technology on Aerospace Chemical Power Laboratory (No. STACPL220191B02), and State Key Laboratory of Materials Processing and Die & Mould Technology at Huazhong University of Science and Technology (No. P2021-010). We also thank the Analytical and Testing Center of WUT for the help with carrying out XRD, FTIR, and FESEM analyses.

References

(1) Chen, W.; Zhuang, Y.; Wang, L.; Lv, Y.; Liu, J.; Zhou, T. L.; Xie, R. J. Color-Tunable and High-efficiency Dye-encapsulated Metal-organic Framework Composites Used for Smart White-light-emitting Diodes. *ACS Appl. Mater. Interfaces.* **2018,** 10, 18910-18917.

(2) Cho, J.; Park, J. H.; Kim, J. K.; Schubert, E. F. White Light-emitting Diodes: History, Progress, and Future. *Laser Photonics Rev.* **2017**, 1600147, 1-17.

(3) Schubert, E. F.; Kim, J. K. Solid-state Light Sources Getting Smart. *Science.* **2005**, 308, 1274-1278.

(4) Lustig, W. P.; Shen, Z.; Teat, S. J.; Javed, N.; Velasco, E.; O'Carroll, D. M.; Li, J. Rational Design of a High-efficiency, Multivariate Metal-organic Framework Phosphor for White LED Bulbs. *Chem. Sci*. **2020**, 11, 1814-1824.

(5) Tang, Y.; Wu, H.; Cao, W.; Cui, Y.; Qian, G. Luminescent Metal-organic Frameworks for White LEDs. *Adv. Optical Mater.* **2020**, 2001817,1-14.

(6) Cui, Y.; Song, T.; Yu, J.; Yang, Y.; Wang, Z.; Qian, G. Dye Encapsulated Metal-organic Framework for Warm-white LED with High Color-rendering Index. *Adv. Funct. Mater.* **2015**, 25, 4796-4802.

(7) Radha, E.; Komaraiah, D.; Sayanna, R.; Sivakumar J., Photoluminescence and Photocatalytic Activity of Rare Earth Ions Doped Anatase TiO_2 Thin Films. *J. Lumin.* **2022**, 244, 118727.

(8) Wang, C.; Huang, Y.; Heydari, E.; Yang, X.; Xu, S.; Bai, G. Dual-mode Optical Ratiometric Thermometer Based on Rare Earth Ions Doped Perovskite Oxides with Tunable Luminescence. *Ceram. Int.* **2022**, 48, 12578-12584.

(9) Qiao, J.; Zhang, Z.; Zhao, J.; Xia, Z. Tuning of the Compositions and Multiple Activator Sites toward Single-phased White Emission in $(Ca_{9-x}Sr_x)MgK(PO_4)_7:Eu^{2+}$ Phosphors for Solid-state Lighting. *Inorg. Chem.* **2019**, 58, 5006-5012.

(10) Zhang, H.; Zhou, M.; Wang, H.; Zhao, Y.; Yu, T. Synthesis and Properties of Butterfly-shaped Naphthalimide-based AIE-active Fluorescent Dyes, *Chemical Papers*. **2022**, 76, 2397-2404.

(11) Wen, Y.; Sheng, T.; Zhu, X.; Zhuo, C.; Su, S.; Li, H.; Hu, S.; Zhu, Q. L.; Wu, X. Introduction of Red-green-blue Fluorescent Dyes into a Metal-organic Framework for Tunable White Light Emission. *Adv. Mater.* **2017**, 1700778, 1-8.

(12) Xing, W.; Zhou, H.; Han, J.; Zhou, Y.; Gan, N.; Cuan, J. Dye Encapsulation Engineering in a Tetraphenylethylene-based MOF for Tunable White-light Emission, *J. Colloid Interface Sci.* **2021**, 604, 568-574.

(13) Liu, X. Y.; Xing, K.; Li, Y.; Tsung, C. K.; Li, J. Three Models to Encapsulate Multicomponent Dyes into Nanocrystal Pores: a New Strategy for Generating High-quality White Light. *J. Am. Chem. Soc.* **2019**, 141, 14807-14813.

(14) Mao, L.; Wu, Y.; Stoumpos, C. C.; Wasielewski, M. R.; Kanatzidis, M. G. White-light Emission and Structural Distortion in New Corrugated Two-dimensional Lead Bromide Perovskites. *J. Am. Chem. Soc.* **2017**, 139, 5210-5215.

(15) Dohner, E. R.; Jaffe, A.; Bradshaw, L. R.; Karunadasa, H. I. Intrinsic White-light Emission from Layered Hybrid Perovskites. *J. Am. Chem. Soc.* **2014**, 136, 13154-13157.

(16) Karmakar, A.; Bernard, G. M.; Meldrum, A.; Oliynyk, A. O.; Michaelis, V. K. Tailorable Indirect to Direct Band-gap Double Perovskites with Bright White-light Emission: Decoding Chemical Structure Using Solid-state NMR. *J. Am. Chem. Soc.* **2020**, 142, 10780-10793.

(17) Mao, L.; Wu, Y.; Stoumpos, C. C.; Traore, B.; Katan, C.; Even, J.; Wasielewski, M. R.; Kanatzidis, M. G. Tunable White-light Emission in Single-cation-templated Three Layered 2D Perovskites $(CH_3CH_2NH_3)_4Pb_3Br_{10-x}Cl_x$. *J. Am. Chem. Soc.* **2017**, 139, 11956-11963.

(18) Yang, B.; Han, K. Charge-Carrier Dynamics of Lead-Free Halide Perovskite Nanocrystals. *Acc. Chem. Res.* **2019**, 52, 3188-3198.

(19) Cong, M.; Zhang, Q.; Yang, B.; Chen, J.; Xiao, J.; Zheng, D.; Zheng, T.; Zhang, R.; Qing, G.; Zhang, C.; Han, K. Bright Triplet Self-Trapped Excitons to Dopant Energy Transfer in Halide Double-Perovskite Nanocrystals. *Nano Lett.* **2021**, 21, 8671-8678.

(20) Bai, T.; Wang, X.; Wang, Z.; Ji, S.; Meng, X.; Wang, Q.; Zhang, R.; Han, P.; Han, K.; Chen, J.; Liu, F.; Yang, B. Highly Luminescent One-Dimensional Organic-Inorganic Hybrid Double-Perovskite-Inspired Materials for Single-Component Warm White-Light-Emitting Diodes. *Angew. Chem.* **2023**, 135, e202213240.

(21) Wie, T. V.; Wysocki, E.; McBride, J. R.; Rosenthal, S. J. Bright Cool White Emission from Ultrasmall CdSe Quantum Dots. *Chem. Mater.* **2019**, 31, 8558-8562.

(22) Ghosh, T.; Prasad, E. White-light Emission from Unmodified Graphene Oxide Quantum Dots. *J. Phys. Chem. C.* **2015**, 119, 2733-2742.

(23) Rodriguez, G. S.; Sanchez-Zeferino, R.; Chapa, C.; Alvarez Ramos, M. E. Silica-coated ZnS Quantum Dots for Multicolor Emission Tuning from Blue to White Light. *ACS Appl. Nano Mater*. **2021**, 4, 12180-12187.

(24) Xu, X.; He, H.; Fang, Z.; Lou, H.; Lin, C.; Chen, L.; Ye, Z. Ultrasonication-assisted Ambient-air Synthesis of Monodispersed Blue-emitting $CsPbBr_3$ Quantum Dots for White Light Emission. *ACS Appl. Nano Mater.* **2019**, 2, 6874-6879.

(25) Li, Y.; Wang, Y. Q.; Liu, D.; Gao, Y.; Wang, S. N.; Qiu, H. Dual-emission Ratiometric Fluorescent Probe Based on Lanthanide Functionalized Carbon Quantum Dots for White Light Emission and Chemical Sensing. *ACS Omega*. **2021**, 6, 14629-14638.

(26) Panniello, A.; Di Mauro, A. E.; Fanizza, E.; Depalo, N.; Agostiano, A.; Curri, M. L.; Striccoli, M. Luminescent Oil-soluble Carbon Dots toward White Light Emission: a Spectroscopic Study. *J. Phys. Chem. C*. **2017**, 122, 839-849.

(27) Barman, B. K.; Handegård, Ø. S.; Hernández-Pinilla, D.; Shinde, S. L.; Nagao, T. Transparent Hard Coatings with SiON-encapsulated N-doped Carbon Dots for Complete UV Blocking and White Light Emission. *ACS Appl. Electron. Mater*. **2021**, 3, 3761-3773.

(28) Du, X. D.; Wang, C. C.; Liu, J. G.; Zhao, X. D.; Zhong, J.; Li, Y. X.; Li, J.; Wang, P. Extensive and Selective Adsorption of ZIF-67 towards Organic Dyes: Performance and Mechanism. *J. Colloid Interface Sci*. **2017**, 506, 437-441.

(29) Yao, T.; Dong, G.; Qian, S.; Cui, Y.; Chen, X.; Tan, T.; Li, L. Persistent Luminescence Nanoparticles/Hierarchical Porous ZIF-8 Nanohybrids for Auto-luminescence-free Detection of Dopamine. *Sens. Actuators B Chem.* **2022**, 357, 131470.

(30) Stone, A. E. B. S.; Irgen-Gioro, S.; López-Arteaga, R.; Hupp, J. T.; Weiss, E. A. Encapsulating CdSe/CdS QDs in the MOF ZIF-8 Enhances Their Photoluminescence Quantum Yields in the Solid State. *Chem. Mater*. **2022**, 34, 1921-1929.

(31) Cui, Y.; Yue, Y.; Qian, G.; Chen, B. Luminescent Functional Metal-organic Frameworks. *Chem. Rev*. **2012**, 112, 1126-1162.

(32) Yin, H. Q.; Yin, X. B. Metal-organic Frameworks with Multiple Luminescence Emissions: Designs and Applications. *Acc. Chem. Res*. **2020**, 53, 485-495.

(33) Shu, Y.; Ye, Q.; Dai, T.; Xu, Q.; Hu, X. Encapsulation of Luminescent Guests to Construct Luminescent Metal-organic Frameworks for Chemical Sensing. *ACS Sens.* **2021**, 6, 641-658.

(34) Gong, Q.; Hu, Z.; Deibert, B. J.; Emge, T. J.; Teat, S. J.; Banerjee, D.; Mussman, B.; Rudd, N. D.; Li, J. Solution Processable MOF Yellow Phosphor with Exceptionally High Quantum Efficiency. *J. Am. Chem. Soc.* **2014**, 136, 16724-16727.

(35) Wei, Z.; Gu, Z. Y.; Arvapally, R K.; Chen, Y. P.; McDougald, Jr. R N.; Ivy, J. F.; Yakovenko, A. A.; Feng, D.; Omary, M. A.; Zhou, H. C. Rigidifying Fluorescent Linkers by Metal-organic Framework Formation for Fluorescence Blue Shift and Quantum Yield Enhancement. *J. Am. Chem. Soc.* **2014**, 136, 8269-8276.

(36) Cao, W.; Cui, Y.; Yang, Y.; Qian, G. Dyes Encapsulated Nanoscale Metal-organic Frameworks for Multimode Temperature Sensing with High Spatial Resolution. *ACS Mater. Lett.* **2021**, 3, 1426-1432.

(37) Zhang, Y.; Tan, J. C. Electrospun Rhodamine@MOF/Polymer Luminescent Fibers with a Quantum Yield of over 90%. *iScience.* **2021**, 24, 103035.

(38) Chen, Y.; Yu, B.; Cui, Y.; Xu, S.; Gong, J. Core-shell Structured Cyclodextrin Metal-organic Frameworks with Hierarchical Dye Encapsulation for Tunable Light Emission. *Chem. Mater*. **2019**, 31, 1289-1295.

(39) Glembockyte, V.; Frenette, M.; Mottillo, C.; Durantini, A. M.; Gostick, J.; Strukil, V.; Friščić, T.; Cosa, G. Highly Photostable and Fluorescent Microporous Solids Prepared via Solid-state Entrapment of Boron Dipyrromethene Dyes in a Nascent Metal-organic Framework. *J. Am. Chem. Soc.* **2018**, 140, 16882-16887.

(40) Xiong, T.; Zhang, Y.; Amin, N.; Tan, J. C. A Luminescent Guest@ MOF Nanoconfined Composite System for Solid-State Lighting. *Molecules*. **2021**, 26, 7583.

(41) Yin, J. C.; Chang, Z.; Li, N.; He, J.; Fu, Z. X.; Bu, X. H. Efficient Regulation of Energy Transfer in a Multicomponent Dye-loaded MOF for White-light Emission Tuning. *ACS Appl. Mater. Interfaces.* **2020**, 12, 51589-51597.

(42) Liang, H. W.; Jia, T.; Wang, Z. Z.; Wang, J. Q.; Hou, D. Y.; Wang, L.; Gao, X.; Sun, H. L.; Wang, H. Anti-solvatochromic and Highly Emissive Twisted D-A Structure with Intramolecular Hydrogen Bond. *Mater. Chem. Front.* **2022**, 6, 512-518.

(43) Jian, M.; Liu, B.; Liu, R.; Qu, J.; Wang, H.; Zhang, X. Water-based Synthesis of Zeolitic Imidazolate Framework-8 with High Morphology Level at Room Temperature. *RSC Adv.* **2015**, 5, 48433-48441.

(44) Liu, Q.; Tian, S.; Zhao, X.; Sankar, G. An Enhanced Fluorescent ZIF-8 Film by Capturing Guest Molecules for Light-emitting Applications. *J. Mater. Chem. C*. **2021**, 9, 5819-5826.

(45) Cheng, P.; Hu, Y. H. H_2O-functionalized Zeolitic Zn(2-methylimidazole)$_2$ Framework (ZIF-8) for H_2 Storage. *J. Phys. Chem. C*. **2014**, 118, 21866-21872.

(46) Yuan, X.; Qu, S.; Huang, X.; Xue, X.; Yuan, C.; Wang, S.; Wei, L.; Cai, P. Design of Core-shelled g-C_3N_4@ZIF-8 Photocatalyst with Enhanced Tetracycline Adsorption for Boosting Photocatalytic Degradation. *Chem. Eng. J*. **2021**, 416, 12918.

(47) Noor, T.; Raffi, U.; Iqbal, N.; Yaqoob, L.; Zaman, N. Kinetic Evaluation and Comparative Study of Cationic and Anionic Dyes Adsorption on Zeolitic Imidazolate Frameworks-based Metal Organic Frameworks. *Mate. Res. Express.* **2019**, 6, 125088.

(48) Bhattacharyya, S.; Pang, S. H.; Dutzer, M. R.; Lively, R. P.; Walton, K. S.; Sholl, D. S.; Nair, S. Interactions of SO_2-containing Acid Gases with ZIF-8: Structural Changes and Mechanistic Investigations. *J. Phys. Chem. C*. **2016**, 120, 27221-27229.

(49) Mphuthi, L. E.; Erasmus, E.; Langner, E. H. G. Metal Exchange of ZIF-8 and ZIF-67 Nanoparticles with Fe (II) for Enhanced Photocatalytic Performance. *ACS Omega*. **2021**, 6, 31632-31645.

(50) Wang, Z.; Sun, D.; He, X. Practical Infrared Spectroscopy, Petroleum Industry Press, Beijing. **1982**, pp. 263-268.

(51) Wu, J. G. Modern Fourier Transform Infrared Spectroscopy Technology and Its Application. Scientific and Technical Literature Press, Beijing. **1994**, pp. 573-623.

(52) Hachuła, B.; Nowak, M.; Kusz, J. Crystal and Molecular Structure Analysis of 2-Methylimidazole. *J. Chem. Crystallogr*. **2009**, 40, 201-206.

(53) Guo, Q.; Chen, C.; Zhou, L.; Li, X.; Li, Z.; Yuan, D.; Ding, J.; Wan, H.; Guan, G.; Design of ZIF-8/Ion Copolymer Hierarchically Porous Material: Coordination Effect on the Adsorption and Diffusion for Carbon Dioxide. *Microporous Mesoporous Mater*. **2018**, 261, 79-87.

(54) Tran, T. V.; Nguyen, H.; Le, P. H. A.; Nguyen, D. T. C.; Nguyen, T. T.; Nguyen, C. V.; Vo, D. V. N.; Nguyen, T. D. Microwave-assisted Solvothermal Fabrication of Hybrid Zeolitic-imidazolate Framework (ZIF-8) for Optimizing Dyes Adsorption Efficiency Using Response Surface Methodology. *J. Environ. Chem. Eng*. **2020**, 8, 104189.

(55) Wang, Z.; Zhu, C. Y.; Zhao, H. S.; Yin, S. Y.; Wang, S. J.; Zhang, J. H.; Jiang, J. J.; Pan, M.; Su, C. Y. Record High Cationic Dye Separation Performance for Water Sanitation Using a Neutral Coordination Framework. *J. Mater. Chem. A*. **2019**, 7, 4751-4758.

(56) Ni, W.; Xiao, X.; Geng, W.; Zhang, L.; Li, Y.; Li, N. Controllable Preparation of Amino-functionalized ZIF-8: a Functionalized MOF Material for Adsorbing Congo Red and Eriochrome Black T in Aqueous Solution. *JCIS Open*. **2021**, 3, 100018.

(57) Wang, Z.; Zhu, C. Y.; Mo, J. T.; Fu, P. Y.; Zhao, Y. W.; Yin, S. Y.; Jiang, J. J.; Pan, M.; Su, C. Y. White-light Emission from Dual-way Photon Energy Conversion in a Dye-encapsulated Metal-organic framework. *Angew. Chem. Int. Ed*. **2019**, 58, 9752-9757.

(58) Das, K.; Jain, B.; Patel, H. S. Hydrogen Bonding Properties of Coumarin 151, 500, and 35: The Effect of Substitution at the 7-Amino Position. *J. Phys. Chem. A.* **2006**, 110, 1698-1704.

(59) Yan, W. L.; Han, J.; Jia, H. L.; Shen, K.; Wang, T.; Zheng, H. G. Three Highly Stable Cobalt MOFs Based on "Y"-shaped Carboxylic Acid: Synthesis and Absorption of Anionic Dyes. *Inorg. Chem*. **2016**, 55, 8816-8821.

(60) Mubarekyan, E.; Santore, M. Characterization of Polystyrene Latex Surfaces by the Adsorption of Rhodamine 6G. *Langmuir*. **1998**, 14, 1597-1603.

(61) Gutiérrez, M.; Zhang, Y.; Tan, J. C. Confinement of Luminescent Guests in Metal−Organic Frameworks: Understanding Pathways from Synthesis and Multimodal Characterization to Potential Applications of LG@MOF Systems. *Chem. Rev.* **2022**, 122, 10438-10483

(62) Martínez Martínez, V.; López Arbeloa, F.; Bañuelos Prieto, J.; López Arbeloa, I. Characterization of Rhodamine 6G Aggregates Intercalated in Solid Thin Films of Laponite Clay. 2 Fluorescence Spectroscopy. *J. Phys. Chem. B.* **2005**, 109, 7443-7450.

(63) Cai, H.; Lu, W.; Yang, C.; Zhang, M.; Li, M.; Che, C. M.; Li, D. Tandem Förster Resonance Energy Transfer Induced Luminescent Ratiometric Thermometry in Dye-encapsulated Biological Metal-organic frameworks. *Adv. Opt. Mater*. **2018**, 1801149.

(64) Tang, Y.; Cao, W.; Yao, L.; Cui, Y.; Yu, Y.; Qian, G. Polyurethane-coated Luminescent Dye@ MOF Composites for Highly-stable White LEDs. *J. Mater. Chem. C.* **2020**, 8, 12308-12313.

(65) Tang, Y.; Xia, T.; Song, T.; Cui, Y.; Yang, Y.; Qian, G. Efficient Energy Transfer within Dyes Encapsulated Metal-organic Frameworks to Achieve High Performance White Light-emitting Diodes. *Adv. Opt. Mater*. **2018**, 6, 1800968.

(66) Jia, Y. Y.; Yin, J. C.; Li, N.; Zhang, Y. H.; Feng, R.; Yao, Z. Q.; Bu, X. H. Crystalline-state Solvent: Metal-organic Frameworks as a Platform for Intercepting Aggregation-Caused Quenching. *Chin. J. Chem*. **2022**, 40, 589-596.

(67) Sapsford, K. E.; Berti, L.; Medintz, I. L. Materials for Fluorescence Resonance Energy Transfer Analysis: Beyond Traditional Donor-Acceptor Combinations. Angew. Chem. Int. Ed. 2006, 45, 4562-4588.